NANO LETTERS

LETTER

pubs.acs.org/NanoLett

Electrothermal Dynamics of Semiconductor Nanowires under Local Carrier Modulation

Deyi Fu,[†,‡,§] Jijun Zou,[†] Kevin Wang,[†,∥] Rong Zhang,[‡,§] Dong Yu,[⊥] and Junqiao Wu*[,†,∥]

[†]Department of Materials Science and Engineering, University of California, Berkeley, California 94720, United States

[‡]Jiangsu Provincial Key Laboratory of Advanced Photonic and Electronic Materials, School of Electronic Science and Engineering, Nanjing University, Nanjing, Jiangsu 210093, China

[§]Nanjing National Laboratory of Microstructures, Nanjing, Jiangsu 210093, China

[∥]Materials Sciences Division, Lawrence Berkeley National Laboratory, Berkeley, California 94720, United States

[⊥]Department of Physics, University of California, Davis, California 95616, United States

Supporting Information

ABSTRACT: Charge transfer, surface/interface, defect states, and internal fields strongly influence carrier statics and dynamics in semiconductor nanowires. These effects are usually probed using spatially resolved scanning current techniques, where charge carriers are driven to move by diffusion force due to a density gradient, drift force due to internal fields, and thermoelectric force due to a temperature gradient. However, in the analysis of experimental data, analytical formulas are usually used which are based on the assumption that a single component of these forces dominates the carrier dynamics. In this work we show that this simplification is generally not justified even in the simplest configurations, and the scanning microscopy data need to be analyzed with caution. We performed a comprehensive numerical modeling of the electrothermal dynamics of free charge carriers in the scanning photocurrent microscopy configuration. The simulation allows us to reveal and predict important, surprising effects that are previously not recognized, and assess the limitation as well as potential of these scanning current techniques in nanowire characterization.

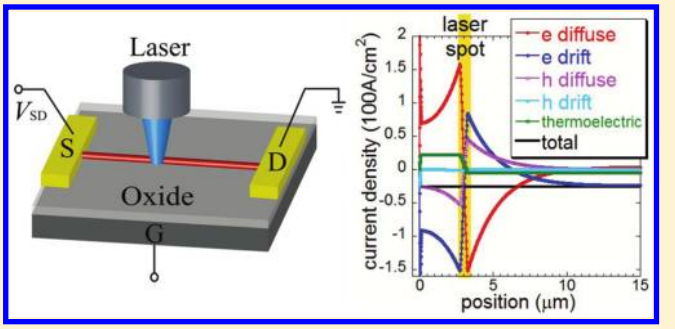

KEYWORDS: Semiconductor nanowires, electrothermal dynamics, scanning photocurrent microscopy, local carrier modulation

Quasi-one-dimensional (1D) semiconductor nanostructures, such as nanowires (NWs), nanobeams, and nanotubes, have attracted tremendous research attention due to their scientific significance as well as potential technological applications.[1−3] Intentional or unintentional internal electric fields often exist in semiconductor NWs caused by electrode contacts, charge transfer, local defects, surface/interface states, doping variations, or band offsets. These fields exert strong influence on the distribution and transport of free charge carriers. As such, it is critical to carefully probe and understand the statics and dynamics of free charge carriers in semiconductor NWs under the influence of local internal fields. In this regard, spatially resolved scanning current techniques have emerged to be powerful tools, in which the electric transport property of a single NW is measured as a function of local carrier density modulation by focused light (scanning photocurrent microscopy), concentrated fields (scanning gate microscopy), or electron beam (electron beam induced current). For example, the scanning photocurrent microscopy (SPCM) combines electrical measurement and local illumination with a focused laser.[4,5] Several groups have used the SPCM to probe effects of electrode contacts, map electronic band bending, evaluate local photovoltaic quantum efficiency, and determine carrier diffusion lengths in NWs.[6−19]

In these experiments, free charge carriers are generally driven to move by diffusion force due to carrier density gradient (chemical potential), drift force due to build-in and/or induced fields (electric potential),[20] and thermoelectric force due to possible temperature gradient.[21,22] To analyze the photocurrent profile, analytical formulas are usually adopted which are based on the assumption that only a single component of these forces dominates the carrier dynamics. However, upon local injection of nonequilibrium carriers in semiconductors, both drift and diffusion currents are always present even in the absence of initial built-in electric fields: large gradients in electron and hole densities are expected which cause diffusion currents; in the meantime, disparity in mobilities of electrons and holes is expected to accumulate local net charges, which induce internal fields and drive drift currents. A comprehensive analysis and understanding of such carrier dynamics in semiconductor NWs subjected to local carrier modulation are still lacking. In this work, we perform a systematic and comprehensive simulation by applying a classical electrothermodynamic model to NWs in the

Received: June 2, 2011
Revised: July 12, 2011
Published: July 26, 2011

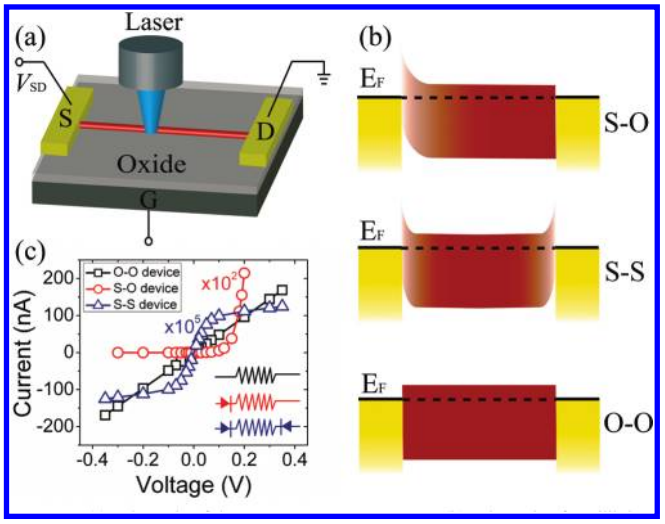

Figure 1. (a) Schematic of the SPCM measurement setup. (b) Schematic of equilibrium band diagrams of three types of NW devices: Schottky−Ohmic (S-O), Schottky−Schottky (S-S), and Ohmic−Ohmic (O-O). An N-type semiconductor NW is assumed. (c) Calculated dark $I-V$ characteristics of the three devices showing the expected rectifying, saturation, and linear behavior, respectively. Note that for clarity, the current for the S-O and S-S devices is multiplied by 10^2 and 10^5, respectively. The parameters used are $L_{NW} = 8\ \mu m$, $N_d = 1 \times 10^{18}\ cm^{-3}$, and $\Phi_{Bn} = 0.5$ V.

SPCM configuration, which allows us to assess the limitation as well as potential of SPCM in NW characterization. The simulation reveals and predicts important, sometimes surprising effects that are previously not recognized. The general results of the simulation are also applicable to other scanning current techniques such as electron beam induced current[23] and scanning gate microscopy,[24] as well as to other geometries such as depth-resolved or cross-sectional scanning of photovoltaic or light-emitting heterostructures.[25]

A typical SPCM setup is shown schematically in Figure 1a, where a NW contacted by two metal electrodes is placed or suspended on top of a substrate. A focused laser beam is locally illuminating the NW. By scanning the laser spot, the photocurrent is recorded as a function of the laser position when the two electrodes (drain and source) are shorted or electrically biased. Optical absorption depth of the NW material is ~300 nm for photon energy ~0.5 eV above the band gap for direct-gap semiconductors, or ~2 eV above the band gap for indirect-gap semiconductors. For NWs with diameters smaller than this absorption depth, the device in Figure 1a can be approximated with a 1D model along the axial direction, where the NW is assumed to be isotropic and homogeneous. The distributions of electric potential and current density are then calculated by solving the coupled Poisson and current continuity equations in 1D. The electric potential $\varphi(x)$ satisfies the Poisson's equation

$$\varepsilon \frac{d^2\varphi(x)}{dx^2} = -|e|(\pm N_{d,a} - n[\varphi(x)] + p[\varphi(x)]) \quad (1)$$

where $N_{d,a}$ is the donor concentration (with positive sign) in N-type semiconductor or acceptor concentration (with negative sign) in P-type semiconductor, which is assumed to be fully ionized at room temperature. The carrier concentrations redistribute in space because the local electric potential modulates carrier population of the conduction and valence bands. Here the full Fermi−Dirac carrier statistics are used to calculate the carrier concentrations such that the calculation is valid across carrier densities ranging from nondegenerate to degenerate, which could be present under intense light illumination or strong band bending.

In steady state, the total current conducted by electrons in a classical semiconductor system is generally given by[22,26]

$$J_n(x) = -\sigma_n(x)\frac{d\varphi(x)}{dx} - eD_n(x)\frac{dn(x)}{dx} - \sigma_n(x)S_n(x)\frac{dT(x)}{dx}$$
$$= -n(x)|e|\mu_n\left[\frac{1}{e}\frac{dE_{Fn}(x)}{dx} + S_n(x)\frac{dT(x)}{dx}\right] \quad (2)$$

where $E_{Fn}(x)$ is the electron quasi Fermi level (electrochemical potential) and μ_n is the electron mobility. Using the Einstein relationship between diffusivity and mobility, the $dE_{Fn}(x)/dx$ term takes into account both the drift ($J_{n,drift}$) and diffusion ($J_{n,diff}$) current components that are driven by electric field ($d\varphi(x)/dx$) and electron density gradient ($dn(x)/dx$), respectively. The $dT(x)/dx$ term is the thermoelectric current component ($J_{n,TE}$), where $S_n(x)$ is the local thermopower (Seebeck coefficient), which is obtained from solution to the Boltzmann transport equation under the relaxation time approximation.[21] We include this term because the focused laser could cause local heating besides nonequilibrium carrier injection. The energy-dependent relaxation time is assumed to follow $\sim E^{\beta}$, where the exponent β is taken to be $-1/2$ assuming acoustic phonon dominated scattering mechanism.[27] A similar treatment is adopted for free hole conduction. The temperature profile $T(x)$ under local laser illumination is obtained through solving the 1D steady-state heat transport equation[28]

$$\frac{d^2T(x)}{dx^2} + \frac{q(x)}{\kappa} = 0 \quad (3)$$

where κ is the thermal conductivity of the NW and q is heat generation rate per unit volume, which is assumed to be constant in the illuminated region and zero otherwise. The heat loss to both the ambient and the substrate is neglected because of the much higher κ of the NW material and poor thermal coupling with the substrate. It should be noted that this assumption is invalid if the NW is tightly surrounded by high-κ dielectrics. We assume that the heat sink through the large metal electrodes at the two ends of the NW is sufficiently fast, such that the temperature there is maintained at the ambient temperature (300 K).

Under photoinjection of electrons and holes, the single equilibrium Fermi level is split into two quasi-Fermi levels ($E_{F,n}(x)$ and $E_{F,p}(x)$). This requires imposing separate current continuity equations for each type of charge carriers

$$\mp\frac{1}{|e|}\frac{dJ_{n,p}(x)}{dx} + R - G = 0 \quad (4)$$

where negative (positive) sign corresponds to electrons (holes). The nonequilibrium electrons and holes are generated solely in the laser illumination area at a rate G, while they recombine throughout the entire NW at a rate R via midgap traps (the Shockley−Read−Hall mechanism)[29] and the Auger process.[30] For the considered system, electron−hole recombination at the NW surface can be normalized into the bulk R through an effective recombination lifetime.[23] At the two ends of the NW, an infinite recombination velocity is assumed across the electrode−semiconductor interface

dx.doi.org/10.1021/nl2018806 |Nano Lett. 2011, 11, 3809–3815

Table 1. Range of Physical Parameters Used in the Simulation

NW material	background doping N_d (cm^{-3})	ambient temperature T_0 (K)	NW length L_{NW} (μm)	NW diameter d_{NW} (nm)	thermal conductivity κ (W/mK)
Si	$10^{14}-10^{18}$	300	4−16	60	25[a]
minority carrier lifetime τ_p (ns)	Schottky barrier height Φ_{Bn} (eV)	laser wavelength λ (nm)	absorption coefficient α (cm^{-1})	laser intensity I_{laser} (kW/cm^2)	laser spot diameter (μm)
4−144	0.6	532	10^4	0.1−300	0.1−1

[a] The value is taken from ref [32] for a ~60 nm diameter Si nanowire.

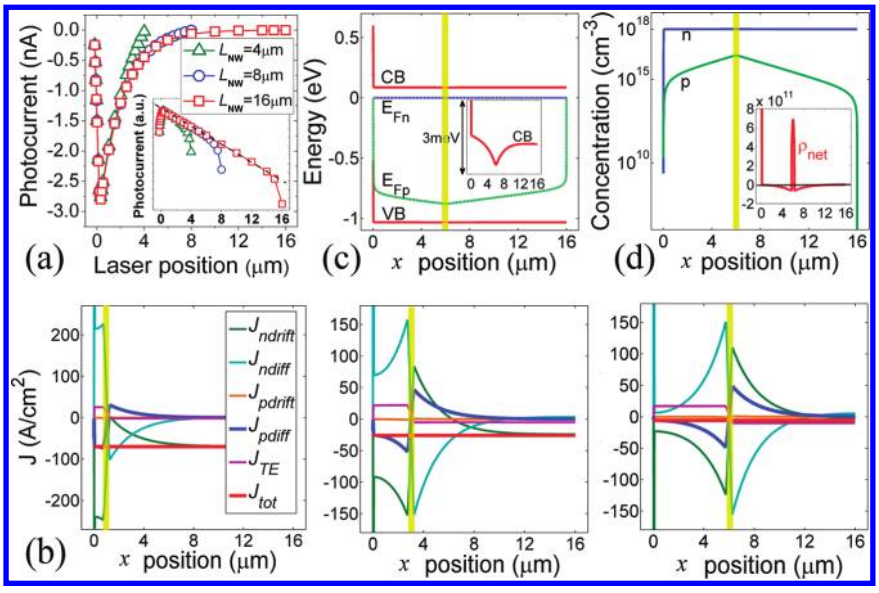

Figure 2. (a) Simulated zero-bias photocurrent profiles of an N-type S-O device with different NW lengths, where the Schottky electrode is on the left-hand side. Inset shows a semilog plot, and a dashed line highlights the exponential decay. (b) Total photocurrent and all current components distribution when the laser is focused at x_{laser} = 1, 3, and 6 μm as indicated by the vertical yellow line (from left to right). Note the total current is continuous throughout the device. Also note the high electron diffusion and drift current (in opposite direction) in the narrow Schottky depletion region (the left-most 50 nm of the NW). (c) Band diagram for x_{laser} = 6 μm. Inset shows the zoom-in conduction band bending. (d) Distribution of majority and minority carriers. Inset shows the net charge distribution. The parameters used are $N_d = 10^{18}$ cm^{-3}, μ_n = 317 $cm^2/(V\,s)$, μ_p = 96 $cm^2/(V\,s)$, τ_p = 16 ns, I_{laser} = 1 kW/cm^2, laser spot size = 0.5 μm (others are taken from Table 1).

(so $E_{F,n} = E_{F,p}$ there). Finally, a finite difference method with non-uniform meshing is used to numerically solve the coupled differential equations self-consistently.[31] To exemplify the simulation, we focus on N-type Si NW devices. Parameters such as carrier effective mass and optical absorption coefficient of Si are obtained from literature, while other material parameters used in the modeling are summarized in Table 1.

Three types of two-terminal NW devices are frequently used in SPCM experiments depending on the nature of the electrical contacts, namely, Schottky−Ohmic (S-O) device, Schottky−Schottky (S-S) device, and Ohmic−Ohmic (O-O) device. Their equilibrium band diagrams (in dark and under zero bias) are schematically illustrated in Figure 1b. At the Schottky contact, the conduction and valence bands of the NW bend upward forming a Schottky barrier, while at the Ohmic contact, an ideal electrical contact is assumed such that the bands are flat. Figure 1c shows dark current−voltage ($I-V$) curves simulated for the three types of devices, where all material parameters are the same except for the contact type. The linear, nonlinear, and rectifying behavior of the $I-V$ curves are expected and well understood. In the following we will discuss these three types of devices separately because, as shown below, the presence of the Schottky barrier drastically affects the charge flow and collection in the NW, resulting in distinct SPCM behaviors.

S-O Device. It will be seen that due to the dominant unidirectional built-in electric field at the Schottky barrier, the S-O device is the simplest type among these three. Figure 2a shows the calculated zero-bias SPCM profiles of S-O devices with different NW lengths, where the doping concentration in the NW is moderately high ($N_d = 10^{18}$ cm^{-3}), and the photoinjection level is relatively low (~10^{16} cm^{-3}). Due to the strong electric field in the space charge region (Figure 2c), negative photocurrent is obtained with a peak located near the Schottky contact (left electrode), away from which the current decays exponentially toward the Ohmic side. Note that the rapid decrease on the left shoulder of the peak is due to shadowing of the laser spot (width 0.5 μm) by the electrode. The photocurrent decay length is several micrometers, much larger than the Schottky depletion width (~50 nm); therefore carrier drift under the initial built-in electric field alone cannot account for the decay.[19] Carrier diffusion (both majority and minority) must play a critical role in determining the total photocurrent. This can be seen more clearly in Figure 2b, which shows all current

dx.doi.org/10.1021/nl2018806 |Nano Lett. 2011, 11, 3809–3815

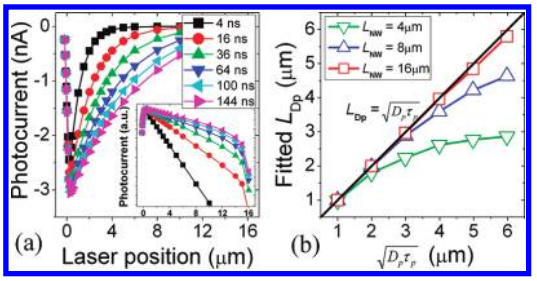

Figure 3. (a) Simulated zero-bias photocurrent profiles of an N-type S-O device under low level photoinjection with different minority carrier lifetime τ_p as shown in the legend. Inset shows the semilog plot. (b) Fitted minority diffusion length L_{Dp} compared with defined minority diffusion length $(D_p\tau_p)^{1/2}$ for three NW lengths (L_{NW}). The parameters used are the same as those used in Figure 2.

components when the laser illuminates different parts along the NW (indicated by the vertical yellow line). From Figure 2b we have the following conclusions: (i) The total thermoelectric current (J_{TE}) is nearly negligible. This is expected as the laser illumination raises the local temperature by only a few kelvin due to its low intensity (half of the laser power is assumed to be transformed into heat at the simulated wavelength). (ii) Minority (hole) drift current ($J_{p,drift}$) is always negligible, whereas majority (electron) drift current ($J_{n,drift}$) is not, which is because $p \ll n$ in this low-level photoinjection condition. The large $J_{n,drift}$ around the laser spot, however, indicates an internal electric field established there. This can be seen in Figure 2c, where the conduction band bending is shown in the inset. The concave band bending is due to the faster diffusion of electrons than holes away from the photoinjection area, which accumulates net positive charges (ρ_{net}) there as shown in Figure 2d. This charge accumulation has been recently experimentally observed in individual CdSe nanowires under local illumination using a combination of electrostatic force microscopy and optical microscopy.[33] The locally induced electric field, albeit much weaker than the built-in field in the Schottky space charge region, has a considerable effect on the current profile because it is in the active (carrier injection) region. (iii) Most importantly, regardless of where the laser illuminates, the hole diffusion current ($J_{p,diff}$) near the Schottky contact region (left side) is always nearly equal to the total current (J_{tot}), while the other current components (mostly $J_{n,diff}$ and $J_{n,drift}$) cancel with each other. This is similar to the equilibrium scenario where $J_{n,diff}$ balances with $J_{n,drift}$ in the space charge region and gives rise to zero J_{tot}. This similarity is not surprising considering that the laser illumination is at a low level injection for electrons ($\Delta n \ll n$ but $\Delta p \gg p$). The nonequilibrium minority carriers (holes) diffuse in both directions; those diffusing toward the left, once reaching the Schottky depletion region, will be efficiently collected due to the strong built-in electric field there. Therefore the total current is limited by the number of holes diffusing to the Schottky electrode. When the laser moves farther away from the Schottky electrode, the holes have to diffuse a longer distance before collection, thus suffering from a higher chance of recombination with electrons and leading to weaker total current. Realizing this, one can fit the right decay shoulder of the SPCM profile in Figure 2a using $\exp(-x/L_{Dp})$, where L_{DP} is the average diffusion length of minority carriers (holes).

By definition, the hole diffusion length is $L_{Dp} = (D_p\tau_p)^{1/2}$, where τ_p is the effective minority carrier lifetime taking into account both bulk and surface recombination and D_p is the

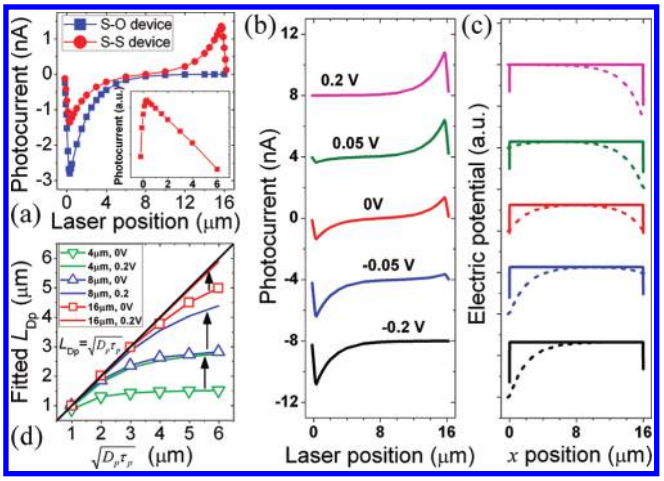

Figure 4. (a) Simulated zero-bias photocurrent profiles of an N-type S-S device under low level photoinjection. An S-O device is also shown for comparison. Inset shows the semilog plot of the S-S device SPCM. (b) Photocurrent of the S-S device under different bias. The right electrode is grounded. The SPCM profiles are offset by 4 nA each for clarity. (c) Electric potential profiles (in dark, solid lines) corresponding to different bias conditions shown in (b). Note the large band bending is limited within the depletion width in the left and right ~50 nm only. Also shown for comparison is the line shape of integrating the photocurrent in (b) over x (dashed lines). (d) Fitted minority diffusion length L_{Dp} compared with defined minority diffusion length $(D_p\tau_p)^{1/2}$ for three NW lengths (L_{NW}) and two different biases (V). The parameters used are same as those used in Figure 2 except the contact type.

diffusion coefficient. Using the mobility of Si at the simulated doping level evaluated from a semiempirical relation,[34] we calculated several SPCM profiles (Figure 3a) as a function of τ_p for a 16 μm long device. As can be seen, the magnitude of the photocurrent is reduced when τ_p becomes shorter. More importantly, for shorter τ_p, the photocurrent decays much faster, resulting in a deeper slope in the semilog plot. By fitting $\exp(-x/L_{Dp})$ to these photocurrent profiles, we obtained the "measured" diffusion length of minority carriers. In Figure 3b, this "measured" L_{Dp} is compared with $(D_p\tau_p)^{1/2}$ directly calculated from the modeling parameters. In analysis of SPCM experimental results, the L_{Dp} extracted from fitting is typically assumed to be an accurate measure of $(D_p\tau_p)^{1/2}$.[12] However, it is found that at large L_{Dp} (or long τ_p), these two start to deviate significantly from each other, and this deviation becomes more serious for shorter NW devices. Furthermore, for large L_{Dp} or short devices, the fitting method always underestimates the real minority carrier diffusion length. Therefore, a long NW device ($L_{NW} > \sim 2L_D$) is needed for accurate determination of the minority L_D. The SPCM profiles of the S-O device as a function of other parameters, such as bias, laser intensity, laser spot size, and Schottky barrier height, are also simulated and shown in the Supporting Information. It is found that variations in these parameters, which could be present in experiments, do not affect the basic conclusions drawn above.

S−S Device. An S-S device can be considered as two S-O devices connected back-to-back, and therefore their SPCM behaviors are expected to be similar, as can be seen from Figure 4a where the profile of an S-O device with the same parameters is also shown for comparison. As expected, the photocurrent of the S-S device is antisymmetric with respect to the middle of the NW and its magnitude is reduced from that of the S-O device, due to additional blocking effect at the other

dx.doi.org/10.1021/nl2018806 |Nano Lett. 2011, 11, 3809–3815

Schottky barrier. The bias dependence of the SPCM of the S-S device is shown in Figure 4b. As can be seen, the photocurrent peak near the positive electrode gradually shrinks and finally disappears at increasing bias, while the peak near the negative electrode is enhanced. This behavior is consistent with experimental results of Ahn et al.,[7] where a P-type NW device was used instead. The electric potential distribution is shown in Figure 4c. When a bias is applied, the voltage mainly drops near the negative electrode and increases the band bending there. The Schottky depletion width (~50 nm) does not expand much and remains much narrower than the decay length of the photocurrent (>1 μm). The majority of the NW remains in nearly flat band condition despite the voltage bias. This is because the depletion region near the contact is much more resistive than the rest of the NW. In SPCM experiments of S-O or S-S devices, one typically assumes that the total current is dominated by carrier drift and therefore is proportional to local electric field $d\varphi(x)/dx$. Consequently, it is believed that the electric potential $\varphi(x)$ in the NW can be evaluated by integrating the photocurrent over x.[7,11] However, as shown by comparing the real $\varphi(x)$ with the integration of photocurrent in Figure 4c, this "integration" method significantly overestimates the spatial extension of the built-in electric field. This discrepancy is because of the erroneous assumption that the photocurrent is contributed solely by the drift of electrons and holes. Moreover, the method is unable to reveal the residual band bending near the positive electrode at all. The "integration" method is also sometimes used to evaluate internal electric fields arising from local defects or doping variations in SPCM experiments of NWs.[13,14] Our results indicate that this method needs to be used with caution. It should be pointed out, however, that if the Schottky barrier is low enough for thermionic emission or thin enough for carriers to tunnel through, the contact resistance can be negligible and the bias voltage will mainly drop across the body of the NW. In these cases, the external electric field along the NW results in an effective Ohmic−Ohmic device, as will be discussed in detail below.[19]

By fitting the exponential decay shoulder of either peak at zero bias, one can extract the minority carrier diffusion length L_{Dp} as in the case of an S-O device. We show the results in Figure 4d for three devices with different L_{NW}. Similar to the S-O device, the fitted L_{Dp} agrees with $(D_p\tau_p)^{1/2}$ in the S-S device only at small L_{Dp}/L_{NW} ratios. It should be noted that the deviation of the fitted L_{Dp} from $(D_p\tau_p)^{1/2}$ (Figure 4d) is much more serious than in the S-O device (cf. Figure 3b). However, in contrast to the S-O device where the photocurrent decay length is nearly independent of bias (Figure S1c, Supporting Information), in the S-S device it is bias dependent (Figure 4b). Applying a bias to the S-S device suppresses the photocurrent near the positive electrode, whereas L_- obtained from fitting the enhanced photocurrent near the negative electrode is enlarged toward $(D_p\tau_p)^{1/2}$. It should be emphasized that the Schottky barrier height assumed here (0.6 eV) is large so that the bias voltage mainly drops at the contacts. As a result, L_{Dp} can only be partially recovered toward $(D_p\tau_p)^{1/2}$ especially for short devices (Figure 4d), as the photocurrent enhancement at the negative electrode quickly saturates with increasing bias (not shown). Therefore, for SPCM of S−S devices, our modeling results recommend using long device (with large Schottky barrier) and/or applying a voltage bias for more accurate estimation of the effective minority diffusion length.

O-O Device. It is commonly assumed that in O-O devices where space charge and band bending are absent in equilibrium, diffusion will dominate over drift under photoexcitation, such that O-O devices have the ideal configuration for extraction of carrier diffusion lengths.[8] In this section, however, we show that O-O devices are in fact more complicated compared to S-O and S-S devices. This is because mobility mismatch of locally photogenerated electrons and holes develops weak, local potential variation in the system. The thus-established (induced) electric field is much weaker than the built-in electric field at Schottky junctions in S-O or S-S devices and yet is sufficiently strong to drive drift currents that are comparable to diffusion currents.

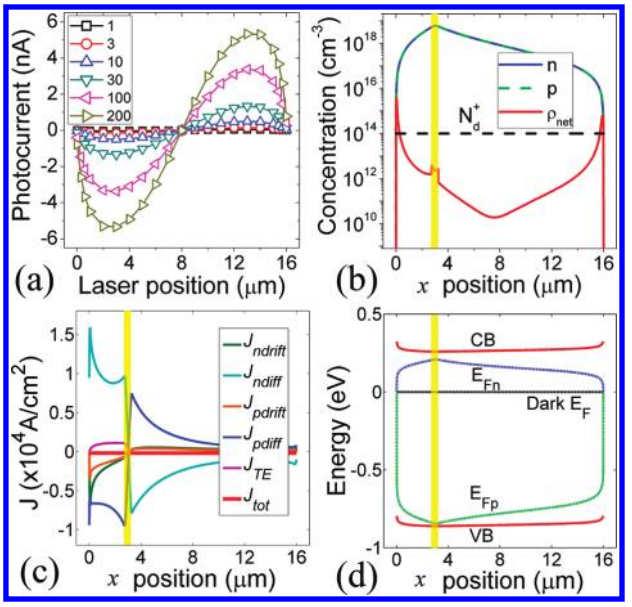

Figure 5. (a) Simulated zero-bias SPCM profiles of an N-type O-O device under different laser intensities as shown in the legend (units: kW/cm^2). (b) Distribution of ionized donor, electron, hole, and net charge densities, (c) current components distribution, and (d) band bending when laser (I_{laser} = 200 kW/cm^2) is illuminating at x_{laser} = 3 μm, the position where the photocurrent peaks as shown in (a). The parameters used are $N_d = 10^{14}$ cm^{-3}, $\tau_p = \tau_n$= 16 ns, laser spot size = 0.5 μm (others are taken from Table 1). Note that a position-dependent carrier mobility has been considered due to intense laser illumination.

In Figure 5a, we show simulated zero-bias SPCM profiles for an N-type O-O device under illumination with a wide range of laser intensities, which correspond to photoinjection level ranging from moderate ($\Delta n = \Delta p \sim n_0 = N_d$) to extremely high ($\Delta n = \Delta p \gg n_0 = N_d$). Two antisymmetric SPCM peaks show up with negative (toward left) photocurrent on the left side and positive photocurrent on the right side. This appears to oppose the common wisdom that when the laser is exciting closer to the left electrode, the net current would be positive, because when carriers diffuse away from the photoinjection region, more electrons (with higher mobility) than holes (with lower mobility) could reach the left electrode. However, as discussed above (Figure 2c,d), a weak internal electric field can be induced along the NW axis when charge neutrality is locally broken due to the mismatch between electron and hole mobilities.[33] As shown in Figure 5b, the faster diffusion of electrons causes net positive charges accumulated inside the NW (especially near the two contacts) and the conduction and valence bands to bend concavely with a minimum located at the photoinjection area (Figure 5d). A steady state is reached when the bands bend to the extent that the electron diffusion is no longer dominant

dx.doi.org/10.1021/nl2018806 |Nano Lett. 2011, 11, 3809–3815

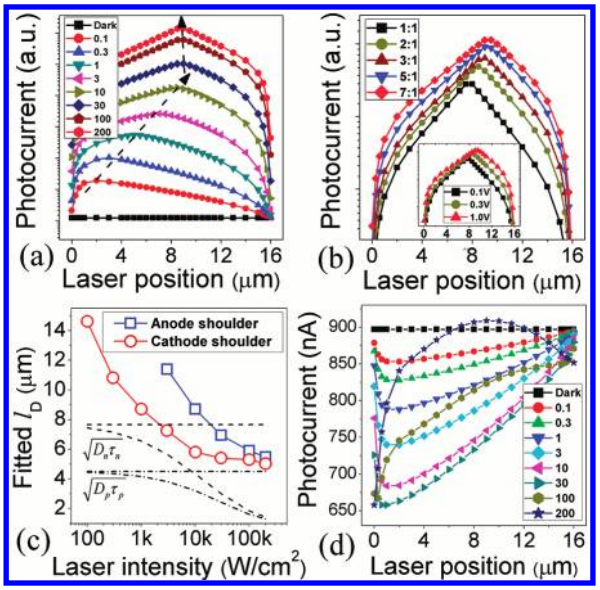

Figure 6. (a) Simulated biased SPCM profiles (log scale) for a lightly doped (N_d = 10^{14} cm^{-3}) N-type O-O device under different laser intensities as shown in the legend (units: kW/cm^2). The bias is fixed at 1 V applied at the left-hand electrode (anode). The dashed arrow indicates the peak shift. (b) Simulated SPCM profiles at 1 V bias under ultrahigh level photoinjection (I_{laser} = 200 kW/cm^2) for different dark electron/hole mobility ratios as shown in the legend. The dark hole mobility is fixed at 488 cm^2/(V s). Inset: SPCM profiles under different biases with the highest dark electron mobility. (c) The decay lengths fitted from the anode and cathode shoulders in (a) as a function of laser intensity. The two dashed (dash-dotted) lines show the upper and lower bound of $(D_n\tau_n)^{1/2}$ ($(D_p\tau_p)^{1/2}$) along the NW, respectively, due to the position-dependent carrier mobility. (d) Simulated SPCM profiles for a moderately highly doped (N_d = 10^{18} cm^{-3}) N-type O-O device under different laser intensities as shown in the legend (units: kW/cm^2) and 1 V bias. A negative photoconductivity is predicted owing to carrier mobility reduction.

compared to the other current components and the net current becomes negative. Note that the induced band bending is much stronger than in the S-O device (cf. Figure 2c). It should be emphasized that the entire system including two external electrodes remains charge neutral, and the net positive charge accumulation in the NW is a local imbalance among $n(x)$, $p(x)$ and the ionized donor N_d^+. However, the weak field is sufficient to cause considerable drift currents ($J_{n,drift}$ and $J_{p,drift}$), which invalidates the assumption of diffusion domination in O-O devices. The distribution of all current components (in short-circuit condition) is shown in Figure 5c, from which we can see that both diffusion and drift currents are remarkable despite the small total current. Therefore, the attempt to fit the zero-bias SPCM assuming a diffusion-only electrodynamic process is unjustified. We note that when the faster carriers are holes instead of electrons, the zero-bias SPCM profile would switch sign from that shown in Figure 5a (see Supporting Information). The O-O devices under moderate-to-high levels of injection at zero bias can thus be used to determine the faster carriers in the NW.

It is intriguing to investigate the SPCM profile of O-O devices under voltage bias, as experimentally carried out by Gu et al. on intrinsic (slightly n-type) CdS NWs.[8] Figure 6a shows the biased SPCM profiles (in semilog scale) under different laser intensities. When the photoinjection level increases from moderate (0.1 kW/cm^2) to ultrahigh (200 kW/cm^2), the photocurrent peak first moves from near the anode (left electrode) toward the cathode (right electrode) and then slightly shifts back toward the middle as indicated by the dashed arrows. Under high-level injection for a biased O-O device, the photocurrent peak should be located where the total current switches from being limited by electron current (electrons reaching the anode) to being limited by hole current (holes reaching the cathode),[8] which depends on the relative mobility of electrons and holes. It should be pointed out that in the modeling we have considered mobility reduction due to lattice and carrier−carrier scatterings which become significant at high injection levels.[34] Therefore the mobilities of both electrons and holes are no longer constant along the NW because of the variation in local temperature and carrier densities. At very high laser intensities, mobilities of electrons (originally faster carrier) and holes are reduced to a level that is comparable to each other, and therefore the peak shifts back toward the middle point. If we artificially increase the dark electron mobility while fixing the hole mobility as shown in Figure 6b, the peak position shifts closer to the cathode (hole collector). In the inset we show the bias dependence of the SPCM with the largest mobility mismatch (μ_n:μ_p = 7:1). As the bias increases, the peak intensity increases and its position shifts toward the cathode. These results are qualitatively consistent with the experimental results of Gu et al. However, we note that the two shoulders of the peak do not exhibit clear linearity as in S-O and S-S devices (cf. Figures 3a and 4a), again implying a complicated carrier transport process not solely governed by carrier diffusion, and therefore cannot be used to directly extract the diffusion parameters. If one forces to fit the nearly linear segments in Figure 6a using the exponential decay function, a light-intensity dependent decay length would be obtained. As shown in Figure 6c, with increasing laser intensity, the decay lengths fitted from both shoulders decrease: the one fitted to the anode shoulder is always larger than the one fitted to the cathode shoulder, but they appear to merge into each other under extremely high level photoinjection. The upper and lower bounds of $(D_n\tau_n)^{1/2}$ and $(D_p\tau_p)^{1/2}$ are shown in Figure 6c. There is no obvious correlation between the fitted SPCM decay lengths and $(D_n\tau_n)^{1/2}$ or $(D_p\tau_p)^{1/2}$, further testifying to a diffusion drift coupled carrier transport process. The carrier dynamics can be better understood by looking into the band bending and current distribution as shown in the Supporting Information (Figure S3).

Finally we also simulated the biased SPCM for an O-O device with much higher doping concentration (N_d = 10^{18} cm^{-3}) under low-to-moderate injection levels as shown in Figure 6d. The dark current is also shown for comparison. When the laser is on, a negative photoconductivity is predicted for this high-doping device, in contrast to the low-doping device shown in Figure 6a. When the laser intensity increases, the photocurrent first decreases, until at a certain level of photoinjection it starts to recover. This conduction reduction in the high-doping device can be explained by the reduction in mobilities of both types of carriers due to enhanced lattice and carrier−carrier scatterings under laser illumination coded in the simulation.[34] However, the negative photoconductivity is absent in low-doping devices even under high level photoinjections, because there the increase in carrier density wins over the reduction in mobility. When this mobility reduction is turned off in the simulation, we found monotonic increase of photocurrent with laser intensity for both low and high-doping devices (see Figure S4 in Supporting Information). We should emphasize that for S-O and S-S devices

dx.doi.org/10.1021/nl2018806 |Nano Lett. 2011, 11, 3809–3815

where we only consider low level photoinjection, the mobility reduction effect is negligible so that position-independent mobilities were used in the simulation.

In summary, we have performed a comprehensive electrothermodynamic modeling of semiconductor NWs under local injection of nonequilibrium carriers. The simulation reveals and predicts important effects that are previously not recognized or appreciated and evaluates the validity of hypotheses that are routinely assumed in analyzing experiments of scanning photocurrent microscopy. The main conclusions are: (i) Schottky−Ohmic and Schottky−Schottky devices can be used to measure minority (but not majority) carrier diffusion length; in this application, devices with long NWs and/or electrically biased devices are recommended for an accurate assessment. (ii) Internal built-in electric potential cannot be determined by integrating the photocurrent because of the nonlocal nature of minority carrier diffusion. An attempt to do so would significantly overestimate the space broadening of the internal field and overlook spots of weaker internal fields. (iii) Ohmic−Ohmic devices can, in fact, have significant drift currents comparable to diffusion currents even in the absence of bias. This invalidates the assumption that carrier diffusion dominates transport process in this type of device. Mobility mismatch of charge carriers in bipolar conduction accumulates local net charges and, in the case of voltage bias, leads to voltage drop mostly in the end of the NW farther from the photoinjection region (see Supporting Information). Under high level photoinjection, it is more meaningful to discuss the two types of carriers as faster carrier and slower carrier, rather than majority carrier and minority carrier. (iv) For high-doping NW devices under low-to-moderate levels of injection, we predict a negative photoconductivity due to mobility reduction by enhanced carrier−lattice and intercarrier scatterings under illumination. We also note that for NWs with low thermal conductivity under high-level photoinjection, considerable thermoelectric current may also arise and should be taken into account in analyzing the total photocurrent.

■ ASSOCIATED CONTENT

Supporting Information. SPCM profiles of S-O devices as a function of different additional parameters, SPCM profiles of an O-O device with holes as faster carriers, and band bending and current distribution in a biased O-O device. This material is available free of charge via the Internet at http://pubs.acs.org.

■ AUTHOR INFORMATION

Corresponding Author
*E-mail: wuj@berkeley.edu.

■ ACKNOWLEDGMENT

This work was supported by the Laboratory Directed Research and Development Program of Lawrence Berkeley National Laboratory under U.S. Department of Energy Contract No. DE-AC02-05CH11231. D. Fu and R. Zhang acknowledge support by Special Funds for Major State Basic Research Project (Grant No. 2011CB301901) and the National Nature Science Foundation of China (Grant No. 60990311). D. Fu also acknowledges the special support of the Graduate Student Research Innovation Project of Jiangsu Province of China (Grant No. CX09B_009Z). We thank Professor Lincoln Lauhon for helpful discussions.

■ REFERENCES

(1) Lu, W.; Xiang, J.; Timko, B. P.; Wu, Y.; Lieber, C. M. *Proc. Natl. Acad. Sci. U.S.A.* **2005**, *102*, 10046–10051.
(2) Li, Y.; Qian, F.; Xiang, J.; Lieber, C. M. *Mater. Today* **2006**, *9*, 18–27.
(3) Hochbaum, A. I.; Yang, P. *Chem. Rev.* **2010**, *110*, 527–546.
(4) Balasubramanian, K.; Fan, Y.; Burghard, M.; Kern, K.; Friedrich, M.; Wannek, U.; Mews, A. *Appl. Phys. Lett.* **2004**, *84*, 2400–2402.
(5) Gu, Y.; Kwak, E. S.; Lensch, J. L.; Allen, J. E.; Odom, T. W.; Lauhon, L. J. *Appl. Phys. Lett.* **2005**, *87*, 043111.
(6) Balasubramanian, K.; Burghard, M.; Kern, K.; Scolari, M.; Mews, A. *Nano Lett.* **2005**, *5*, 507–510.
(7) Ahn, Y.; Dunning, J.; Park, J. *Nano Lett.* **2005**, *5*, 1367–1370.
(8) Gu, Y.; Romankiewicz, J. P.; David, J. K.; Lensch, J. L.; Lauhon, L. J. *Nano Lett.* **2006**, *6*, 948–952.
(9) Gu, Y.; Romankiewicz, J. P.; David, J. K.; Lensch, J. L.; Lauhon, L. J.; Kwak, E. S.; Odom, T. W. *J. Vac. Sci. Technol.* **2006**, *24*, 2172–2177.
(10) Freitag, M; Tsang, J. C.; Bol, A.; Yuan, D.; Liu, J.; Avouris, P. *Nano Lett.* **2007**, *7*, 2037–2042.
(11) Ahn, Y.; Tsen, A. W.; Kim, B.; Park, Y. W.; Park, J. *Nano Lett.* **2007**, *7*, 3320–3323.
(12) Kelzenberg, M. D.; Turner-Evans, D. B.; Kayes, B. M.; Filler, M. A.; Putnam, M. C.; Lewis, N. S.; Atwater, H. A. *Nano Lett.* **2008**, *8*, 710–714.
(13) Allen, J. E.; Hemesath, E. R.; Lauhon, L. J. *Nano Lett.* **2009**, *9*, 1903–1908.
(14) Allen, J. E.; Perea, D. E.; Hemesath, E. R.; Lauhon, L. J. *Adv. Mater.* **2009**, *21*, 3067–3072.
(15) Koren, E.; Rosenwaks, Y.; Allen, J. E.; Hemesath, E. R.; Lauhon, L. J. *Appl. Phys. Lett.* **2009**, *95*, 092105.
(16) Putnam, M. C.; Turner-Evans, D. B.; Kelzenberg, M. D.; Boettcher, S. W.; Lewis, N. S.; Atwater, H. A. *Appl. Phys. Lett.* **2009**, *95*, 163116.
(17) Soudi, A.; Dhakal, P.; Gu, Y. *Appl. Phys. Lett.* **2010**, *96*, 253115.
(18) Kim, C.; Lee, H.; Cho, Y.; Kang, K.; Jo, M. *Nano Lett.* **2010**, *10*, 2043–2048.
(19) Graham, R.; Miller, C.; Oh, E.; Yu, D. *Nano Lett.* **2011**, *11*, 717–722.
(20) Gregg, B. A.; Hanna, M. C. *J. Appl. Phys.* **2003**, *93*, 3605–3614.
(21) Cai, J.; Mahan, G. D. *Phys. Rev. B* **2006**, *74*, 075201.
(22) Fu, D.; Levander, A. X.; Zhang, R.; Ager, J. W., III; Wu, J. *Phys. Rev. B* **2011**, *84*, 045205.
(23) Allen, J. E.; Hemesath, E. R.; Perea, D. E.; Lensch-Falk, J. L.; Li, Z. Y.; Yin, F.; Gass, M. H.; Wang, P.; Bleloch, A. L.; Palmer, R. E.; Lauhon, L. J. *Nat. Nanotechnol.* **2008**, *3*, 168–173.
(24) Bachtold, A.; Fuhrer, M. S.; Plyasunov, S.; Forero, M; Anderson, E. H.; Zettl, A.; McEuen, P. L. *Phys. Rev. Lett.* **2000**, *84*, 6082–6085.
(25) Brown, G.; Faifer, V.; Pudov, A.; Anikeev, S.; Bykov, E.; Contreras, M.; Wu, J. *Appl. Phys. Lett.* **2010**, *96*, 022104.
(26) Gurevich, Y. G.; Titov, O. Y.; Logvinov, G. N.; Lyubimov, O. I. *Phys. Rev. B* **1995**, *51*, 6999–7004.
(27) Rowe, D. M. *CRC Handbook of Thermoelectrics*; CRC Press, Inc.: Boca Raton, FL, 1994.
(28) Sucec, J. *Heat Transfer*; Simon & Schuster, Inc.: New York, 1975.
(29) Fossum, J. G. *Solid-State Electron.* **1976**, *19*, 269–277.
(30) Dziewior, J.; Schmid, W. *Appl. Phys. Lett.* **1977**, *31*, 346–348.
(31) Engl, W. L.; Dirks, H. K.; Meinerzhagen, B. *Proc. IEEE* **1983**, *71*, 10–33.
(32) Hochbaum1, A. I.; Chen, R.; Delgado, R. D.; Liang, W.; Garnett, E. C.; Najarian, M.; Majumdar, A.; Yang, P. *Nature* **2008**, *451*, 163–167.
(33) Schäfer, S.; Wang, Z.; Zierold, R.; Kipp, T.; Mews, A. *Nano Lett.* **2011**, *11*, 2672–2677.
(34) Dorkel, J. M.; Leturcq, Ph. *Solid-State Electron.* **1981**, *24*, 821–825.

Supporting information for "Electrothermal Dynamics of Semiconductor Nanowires under Local Carrier Modulation"

D. Fu [1, 2, 3], J. Zou [1] , K. Wang [1, 4], R. Zhang [2,3], D. Yu [5] and J. Wu [1,4]

[1] Department of Materials Science and Engineering, University of California, Berkeley, CA 94720, USA

[2] Jiangsu Provincial Key Laboratory of Advanced Photonic and Electronic Materials, School of Electronic Science and Engineering, Nanjing University, Nanjing, Jiangsu 210093, China

[3] Nanjing National Laboratory of Microstructures, Nanjing, Jiangsu 210093, China

[4] Materials Sciences Division, Lawrence Berkeley National Laboratory, Berkeley, CA 94720, USA

[5] Department of Physics, University of California, Davis, CA 95616, USA

*To whom correspondence should be addressed. Email: wuj@berkeley.edu

1. SPCM profiles of S-O device as a function of different additional parameters

We simulated the effects of additional parameters on the SPCM profile of an S-O device and the results are shown in Fig. S1. An 8-μm long N-type device with moderately-high doping concentration (N_d = 10^{18} cm^{-3}) was chosen as an example. We first simulated for different laser intensities as shown in Fig. S1(a), where the photo-injection level increases from low ($\Delta n = \Delta p << n_0 = N_d$) to moderately high ($\Delta n = \Delta p > n_0 = N_d$). Here the carrier mobility is treated as position-dependent due to lattice and carrier-carrier scatterings under local laser illumination, which only becomes significant at high injection levels.[1] For S-O devices, different Schottky barrier heights could be encountered depending on the specific contact metal and fabrication conditions. The results are shown in Fig. S1(b). As expected, lower barriers yield weaker photocurrents. However, the photocurrent decay length (slope in inset of Fig. S1(b)) remains largely unchanged, which means that the extracted minority diffusion length

from fitting is intrinsic to the NW. Then we simulated SPCM profiles under different biases as shown in Fig. S1(c). As can be seen, the photocurrent decay length is also independent of bias, which is consistent with experiment results reported by Kelzenberg et al.[2] Therefore, applying a voltage bias can not improve the accuracy in evaluating L_{Dp} in the S-O device, in contrast to S-S device. Finally, SPCM profiles using different laser spot sizes were simulated and shown in Fig. S1(d). It can be seen that the photocurrent decay length is also independent of laser spot size, further verifying its intrinsic nature in the S-O device. However, smaller laser spot has higher spatial resolution.

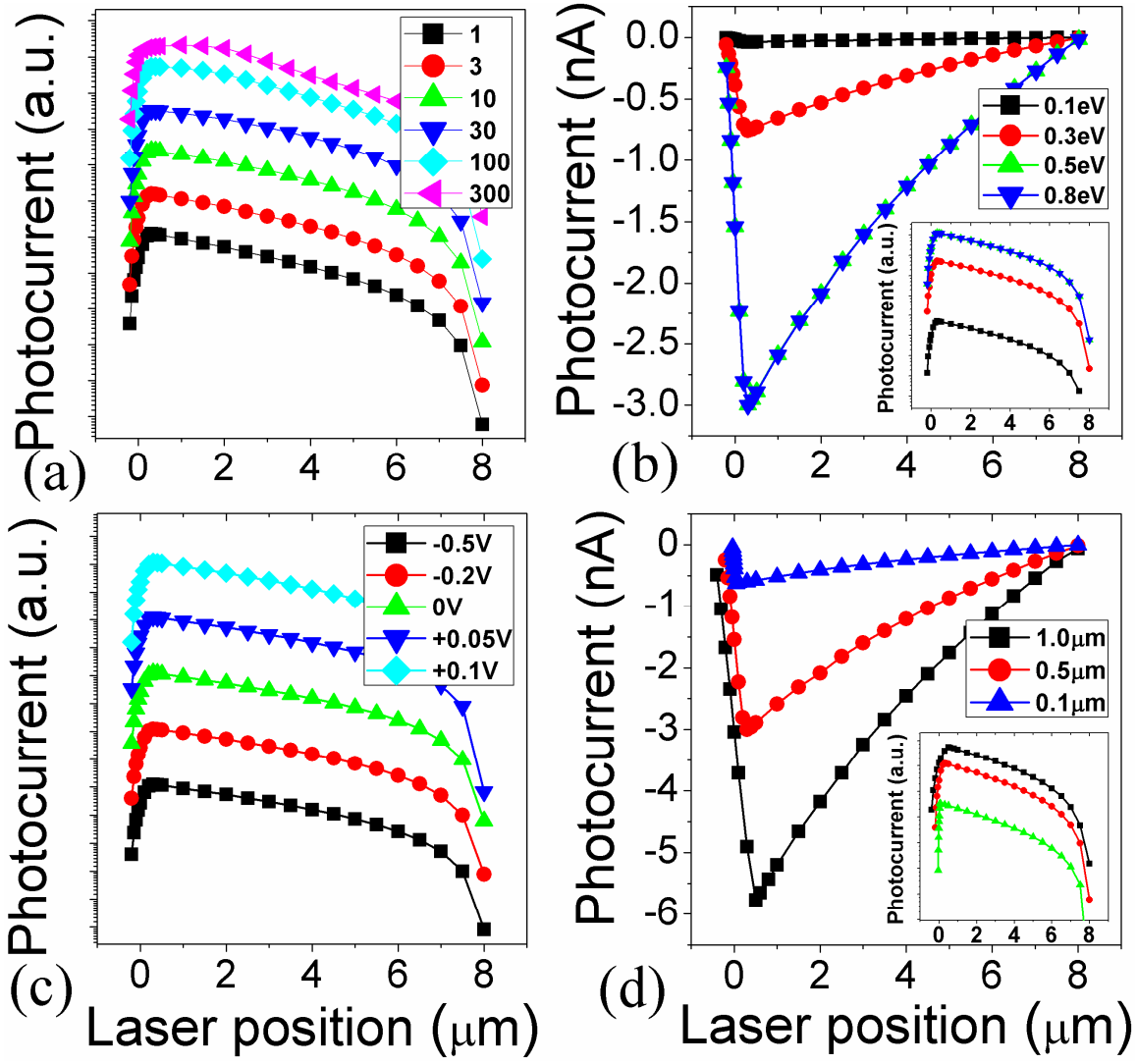

Figure S1. Simulated SPCM profiles for a moderately-high doping (N_d = 10^{18} cm^{-3}) N-type S-O device. (a) SPCM (on log scale) under different laser intensities as shown in the legend (units: kW/cm^2), (b) with different Schottky barrier heights, (c) under different biases (profiles are offset from each other for clarity), and (d) using laser spots with different diameters. Note that for each plot, only one parameter is varied while all others are fixed. In (a), (b) and (d), the bias voltage is zero.

2. SPCM profiles of O-O device with holes as faster carriers

For Si, electrons always have higher mobility than holes. To illustrate the critical role of mobility mismatch between electrons and holes, we artificially set holes as faster carriers (i.e. have a higher mobility) in an N-type O-O device. In Fig. S2(a), we first show the zero-bias SPCM profile for such a device (squares) under high level photo-injection condition. The same device with higher electron mobility (circles) is also shown for comparison. When the carrier mobility ratio switches, the zero-bias SPCM profile switches sign (cf. Figure 5a). This can be understood in a similar way as discussed in the text in terms of band bending (Fig. S2(b)) caused by the mobility mismatch. Although the induced electric field is relatively weak, it is sufficient to cause considerable drift currents (J_{ndrift} and J_{pdrift}) as shown in Fig. S2(c), which invalidates the assumption of diffusion domination in O-O devices. Finally, we simulated the biased SPCM profiles for different dark hole/electron mobility ratios as shown in Fig. S2(d). We artificially increased the dark hole mobility while fixing the dark electron mobility, and found that the peak position shifts closer to the anode (left electrode, i.e. electron collector) when the hole mobility increases. In the inset we show the bias dependence of the SPCM with the largest hole mobility. As the bias increases, the peak intensity increases and its position shifts toward the anode. These results are well expected as discussed in the text due to the fact that holes have higher mobility than electrons. As a result, the O-O devices under

moderate-to-high levels of injection can be used to determine the faster carriers in the NW.

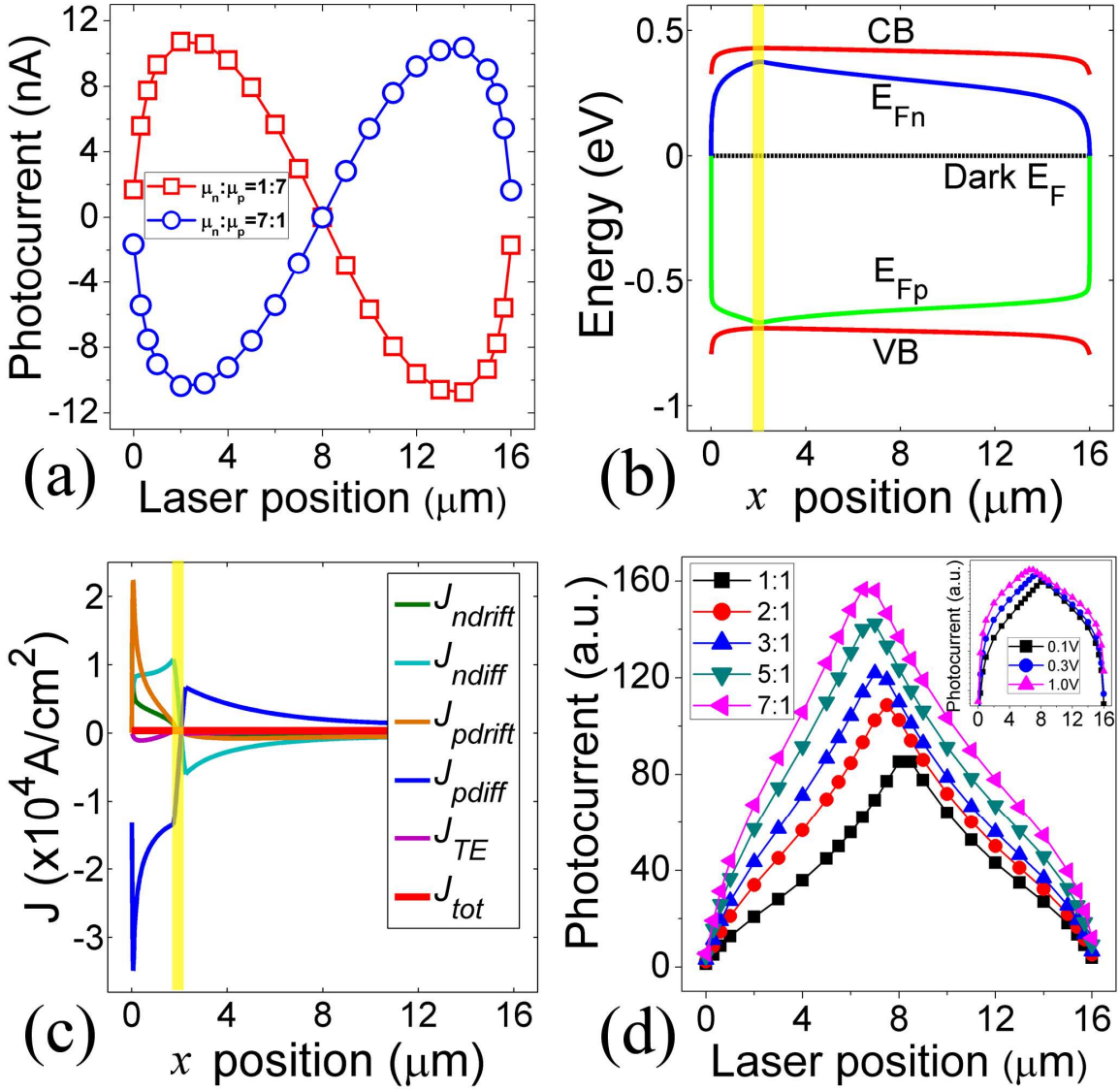

Figure S2. (a) Simulated zero-bias SPCM profile of a lightly doped (N_d = 10^{14} cm^{-3}) N-type O-O device with higher hole mobility under high-level photo-injection (I_{laser} = 200kW/cm^2). The same device with higher electron mobility is also shown for comparison. (b) Band bending and (c) current components distribution when laser is illuminating at x_{laser} = 2 μm, the position where the photocurrent peaks as shown in (a). (d) Simulated SPCM profiles for different dark hole/electron mobility ratios as shown in the legend at 1V bias. The dark electron mobility is fixed at 488 cm^2/Vs. The laser intensity is set at 200kW/cm^2. Inset: SPCM profiles at different biases with highest hole mobility.

3. Band bending and current distribution in biased O-O device

The carrier dynamics in O-O devices can be better understood by looking into the band bending and current distribution as shown in Fig. S4. It can be seen that the bias voltage mostly drops near the two electrodes, while the bands remain almost flat near the photo-injection region. As shown in Figure 5d in the main text for a zero-biased NW under local illumination, the conduction and valence bands are already depleted near the two electrodes, therefore they are more resistive compared to the rest of the NW especially the photo-injection region where high density of free carriers are being generated. When a bias is applied, it is thus expected that the voltage drop (thus band bending) will mostly occur near the two electrodes rather than the photo-injection region.[8,9] It is also noticed that the position of laser injection influences the relative band bending at the two ends: stronger band bending occurs near the electrode farther away from the laser spot. This is because the band bending near the closer electrode can be more easily screened by free carriers (electrons at anode or holes at cathode) that are swept there by the bias voltage. The corresponding steady-state current components are depicted in Fig. S4. It is clear that both diffusion and drift currents from both electrons and holes contribute to the total current on a comparable level, thus leading to the complicated SPCM behavior. In addition, the thermoelectric current also becomes appreciable owing to the intense laser illumination. Therefore, these complications need to be considered in the evaluation of carrier diffusion dynamics using O-O type devices.

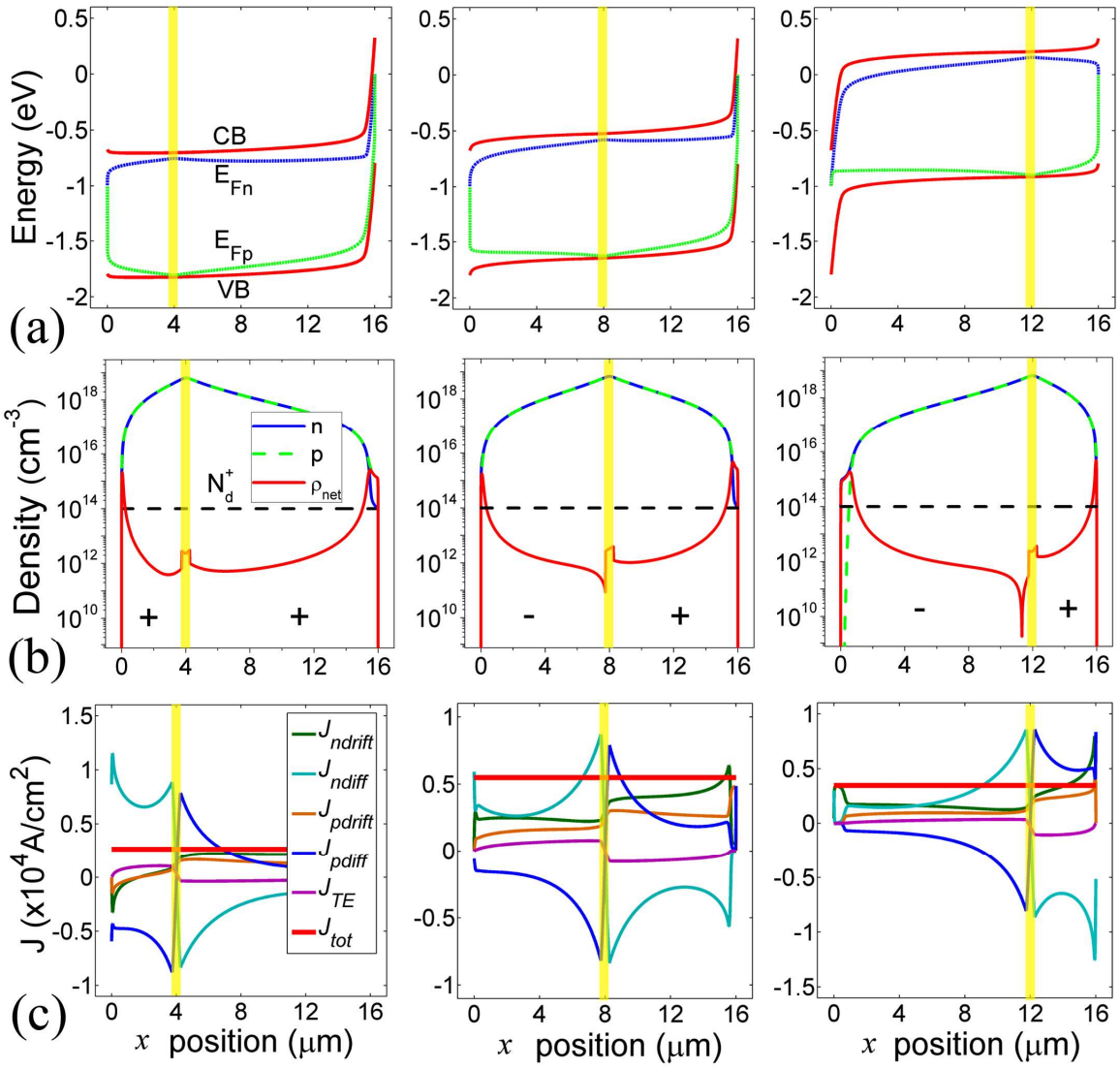

Figure S3. Simulated (a) band diagram, (b) carrier and charge distribution, and (c) current components for a 1V-biased N-type O-O device when laser is illuminating at 4 μm (left), 8 μm (middle) and 12μm (right). The right-hand side electrode is grounded. In (b) the net charge is negative in the left portion and positive in the right portion as denoted in the right two plots. The parameters used are: $N_d = 10^{14}$ cm^{-3}, $\tau_p = \tau_n =$ 16ns, $I_{laser} =$ 200kW/cm^2, laser spot size = 0.5 μm (others are taken from Table 1).

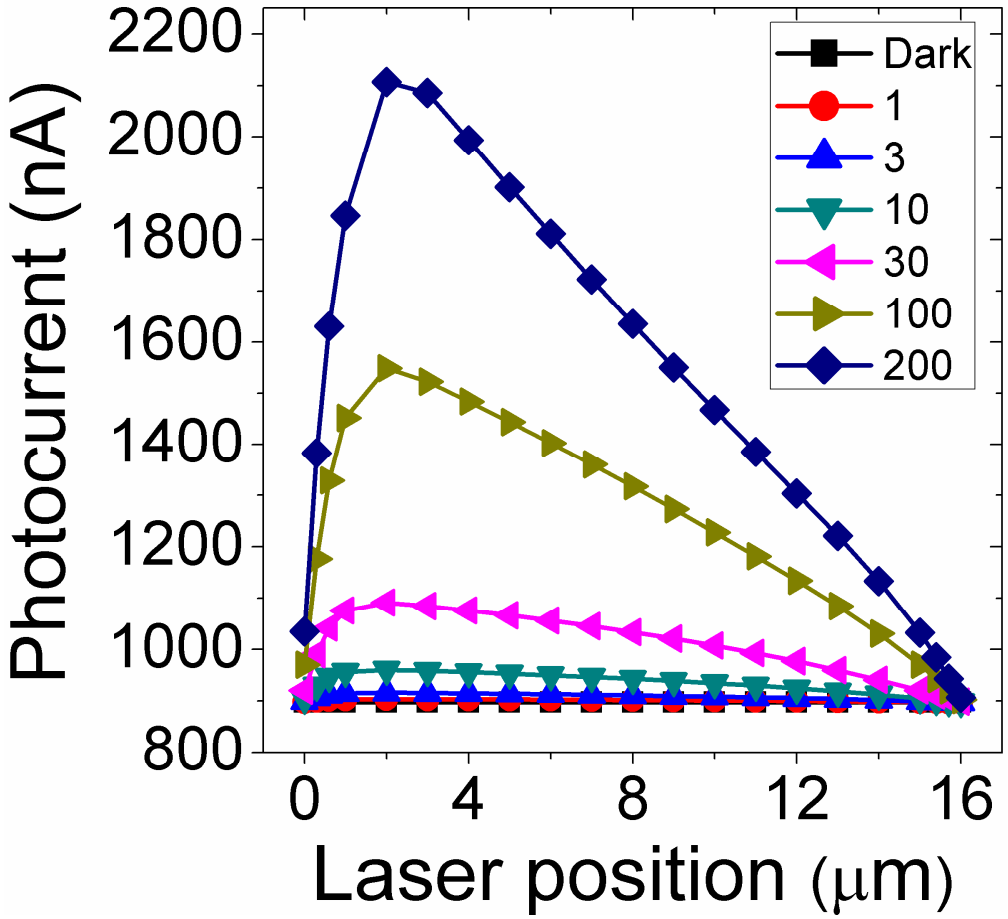

Figure S4. Simulated SPCM profiles for a moderately-high doping (N_d = 10^{18} cm^{-3}) N-type O-O device under different laser intensities as shown in the legend (units: kW/cm^2) and 1V bias. The electron and hole mobility is set to be carrier-density independent throughout the NW.

References to the Supplementary Information

1. Dorkel, J. M.; Leturcq, Ph. *Solid-State Electron.* **1981**, 24, 821-825.

2. Kelzenberg, M. D.; Turner-Evans, D. B.; Kayes, B. M.; Filler, M. A.; Putnam, M. C.; Lewis, N. S.; Atwater, H. A. *Nano Lett.* **2008**, *8*, 710-714.